Pergamon

*Int. J. Solids Structures* Vol. 35, Nos 31–32, pp. 4313–4335, 1998

0020–7683/98 $19.00 + .00

PII: S0020–7683(97)00318–1

# CONTINUUM FRACTURE MECHANICS OF UNIAXIAL COMPRESSION ON BRITTLE MATERIALS

IOANNIS VARDOULAKIS*
National Technical University of Athens, Department of Engineering Science, Zographou 157 73, Greece

JOSEPH F. LABUZ
University of Minnesota, Department of Civil Engineering, Minneapolis, Minnesota 55455, U.S.A.

EURIPIDES PAPAMICHOS and JOHAN TRONVOLL
IKU Petroleum Research Formation Physics Section, N-7034, Trondheim, Norway

(*Received* 15 *November* 1996; *in revised form* 30 *May* 1997)

**Abstract**—A review of the uniaxial compression test on brittle solids is presented. The discussion focuses on the description of the post-peak behavior, where strength softening and fractures propagating mainly in the axial direction are observed. Based on experimental evidence and dimensional analysis, the post-peak axial stress is seen as a function of the axial displacement normalized by the radius of the specimen, and not of its height. Accordingly, a continuum theory of *stress diffusion* is developed that is able to account for size effect. As a practical application of the theory, the bearing capacity of a pillar in a deep mine is considered. © 1998 Elsevier Science Ltd. All rights reserved.

## 1. INTRODUCTION

"... Widespread is the misconception that those who formulate continuum theories believe matter 'really is' continuous, denying the existence of molecules. This is not so. Continuum physics presumes *nothing* regarding the structure of matter. It confines itself to relations among gross phenomena, neglecting the structure of the material on a smaller scale. Whether the continuum approach is justified, in any particular case, is a matter, not for the philosophy or methodology of science, but for the **experimental test**..." (C. Truesdell and W. Noll: *Non-Linear Field Theories of Mechanics*. Encyclopedia of Physics, Vol. III/3, Sect. 3, Springer, 1965).

The uniaxial compression test (Fig. 1) is widely used for mechanical characterization of a great variety of engineering materials such as rock, concrete, and cohesive soil. Here we are interested in the interpretation of experimental results obtained in the phase past the peak load of this test, where strength softening is measured, and fractures propagating mainly in the axial direction are observed. In rock mechanics, the uniaxial compression test has been the subject of extensive research. Wawersik (1968) was among the first to produce reliable experimental data concerning the post-peak phase of this test. Hudson *et al.* (1971) conducted a systematic series of uniaxial compression tests on non-lubricated specimens of Georgia Cherokee marble and determined the influence of specimen geometry and size on the observed strength degradation.

Since the later part of the previous century, from the works of Foeppl, Vicat and Mohr (1900) on uniaxial compression on rock, concrete and masonry, it has been known that platen lubrication is necessary to avoid the serious effect of end friction, which acts as confinement and dramatically influences the strength and failure mode (Fig. 2). Note that Foeppl used "Stearin" as a friction reducer and that Labuz and Bridell (1993) gave a new push to Foeppl's recommendation of a stearic-acid based lubricant, demonstrating that the effect of platen lubrication is paramount. End constraint (developed through platen friction), in relation to softening, was discussed by Drescher and Vardoulakis (1982) and Read and Hegemier (1984) who pointed to the fact that little can be inferred from non-lubricated

* Corresponding author.

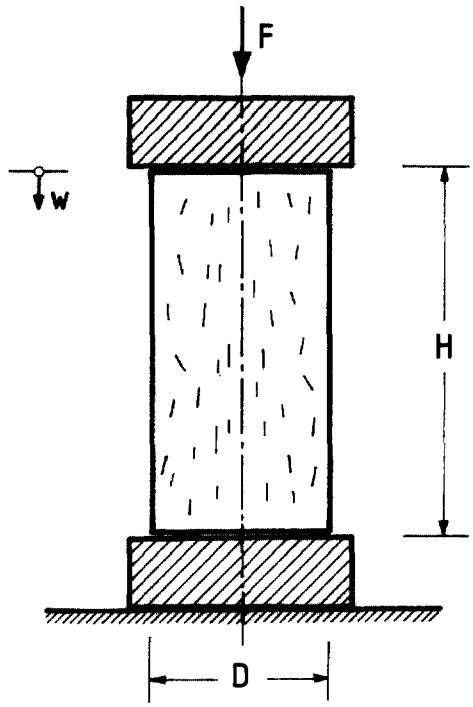


Fig. 1. The uniaxial compression test set-up; definitions of basic geometric and mechanical quantities monitored in this test.

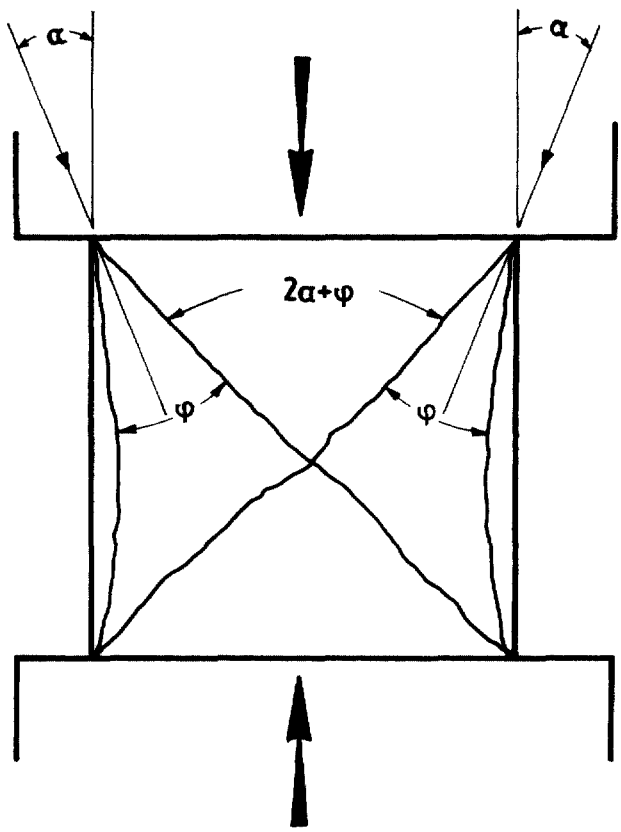


Fig. 2. Reproduction of Mohr's (1900) original drawing in relation to the failure mode observed in uniaxial compression on rock and concrete tests with non-lubricated end platens and his theoretical concept of 'confinement' due to friction.

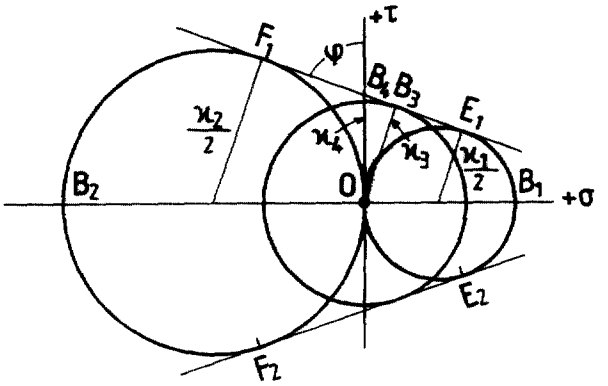


Fig. 3. Reproduction of Mohr's (1900) original drawing for the graphical determination of a linear failure envelope (the well-known Coulomb-Mohr envelope) including uniaxial compression, pure shear and uniaxial tension.

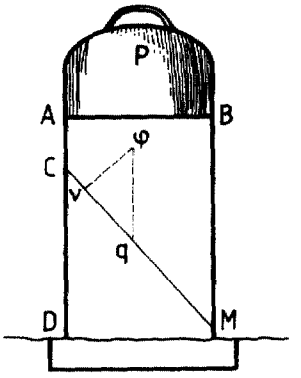


Fig. 4. Reproduction of Coulomb's original drawing concerning the critical failure mechanism in uniaxial compression on rock and the corresponding critical stress combination (see Bell (1973)).

tests especially from those with a small height to diameter ratio. However, short specimens with lubricated ends are preferable to long specimens, because short specimens preclude early development of diffuse bifurcations (barreling or buckling) and support, almost until peak load, homogeneous deformation (Sulem and Vardoulakis, 1990; Chau, 1993; Vardoulakis and Sulem, 1995).

Uniaxial compression together with shear and uniaxial tension are commonly used for the determination of the envelope of attainable stress states in the sense of Mohr (1900) (Fig. 3). According to Mohr's theory, the specimen fails under the combined action of shear and normal stress along characteristic planes. If we replace the pure uniaxial compression test with a triaxial compression test with small confinement, then indeed the specimen fails under shear; that is, moderate confinement suffices to induce failure under shear. The idea of a dominant inclined failure plane in the uniaxial compression test is attributed to Coulomb (Fig. 4) (Bell 1970) and, as already mentioned, is in most cases the result of confinement due to platen friction.

Mohr's theory is not meaningful in those cases where the observed failure mode is the one usually termed as axial splitting. In this case the specimen fails under the formation of a perplex set of fractures, mainly oriented in the axial direction, as is the case whenever proper lubrication is used. (Notice that based on experimental evidence already Mohr (1900) dismissed the hypothetical splitting action of the lubricant.) Fig. 5 (a–c) shows the typical axial splitting failure pattern in a uniaxial compression test with platen lubrication on Berea and Red Wildmoor sandstones, and Dionysos-Pentelicon marble respectively. The fact that failure through axial splitting is incompatible with Mohr's theory can be seen directly from Fig. 3, because any conceivable envelope of the corresponding Mohr circles

will lead to a prediction of failure along some inclined plane (or set of planes), where the critical combination of shear and normal stress will act. Consequently, the corresponding Coulomb-Mohr shear-stress failure criterion (linear or non-linear) is not applicable to uniaxial compression with axial splitting. One could, however, abandon the idea of a shear-stress failure criterion and resort to Saint Venant's tensile-strain failure criterion. It turns out that this proposition is also of little value, since the observed lateral tensile strain at failure in uniaxial compression is typically one order of magnitude larger than the corresponding axial strain at failure in a uniaxial tension test. Notice that only recently was it possible to produce reliable data concerning the uniaxial (direct) tension of marble (Vardoulakis *et al.*, 1998).

Alternatively, one may try to apply Rankine's maximum stress failure criterion (Chen, 1975). From a macroscopic point of view, the assumption of tensile cracks running parallel to the direction of axial compressive stress leads to additional conceptual difficulties. In this case, tensile cracks appear to be propagating under the application of a zero macroscopic stress perpendicular to their plane. Due to macroscopic equilibrium, possible tensile stresses at the grain level must average out to a zero macroscopic stress for planes parallel to the axis of the uniaxially compressed specimen. This means that in order to account for tensile stresses one has to introduce, into the conceptual model for the material, additional structural elements like cracks, grains, grain boundaries etc., which in turn introduce a number of additional unknowns concerning their spatial distribution, average shape and local criteria for their formation and propagation.

As it can be seen from Fig. 6, pure axial splitting is kinematically incompatible with the imposed boundary constraint of rigid end platens. Indeed a 'perfectly' lubricated end platen will push all particles of the tested material at the interface downwards. Axial splitting on the other hand means that the particles move in a horizontal direction. Thus, in limit analysis computations the tested failure mechanisms consist of wedges (bounded by shear fractures), which induce the splitting of the structure, as indicated for the two dimensional case in Fig. 6. Even though three-dimensional models are more elaborate (Chen, 1975; Michalowski, 1985) they work the same way as the two dimensional models. Such mechanisms are relatively easy to analyze and lead directly to the concept of *fragmentation*, that is, to the concept of a combined action of shear and tensile macroscopic fractures.

As already mentioned above, if one wants to apply a local tensile-stress failure criterion for the description of the observed phenomena in uniaxial compression, then one has to abandon macroscopic stress analysis. This leads to the so-called micromechanical considerations. In this case the observed phenomenon of axial splitting in real or model materials is made plausible by using concepts mainly borrowed from linear elastic fracture mechanics (Brace and Bombolakis, 1963; Fairhurst and Cook, 1966; Hoek and Bieniawski, 1965) and from bifurcation theory (Vardoulakis and Papamichos, 1991; Papamichos *et al.*, 1994). Figure 7(a,b) from Hoek (1968) illustrates the idea of tensile cracks propagating from the tip of inclined preexisting flaws under compressive stress. Micromechanical models of distributed microcracks (Hori and Nemet-Nasser, 1986) lead to plausible explanations for the tendency of cracks to orient themselves parallel to the applied far-field compressive stress under little or no confinement. Although computer intensive, this type of modeling provides useful insight into the post-peak behavior of brittle solids in compression (Okui and Horii, 1995). In this paper we are not going to follow that approach.

Direct observations and computer simulations indicate that in order to overcome the constraints imposed mainly by rigid and smooth end platens, brittle solids in uniaxial compression tend to fracture under the formation of randomly distributed vertical and inclined microcracks (Shah and Labuz, 1995; Schlangen and Van Mier, 1994). Van Vliet and Van Mier (1996) using improved experimental techniques of axial displacement control and lubricated end platens as well as variable height to diameter ratios, observed that post-peak data from uniaxial compression experiments on plain concrete suggest a stress-displacement rather than a stress-strain relation. To obtain a unique empirical stress-displacement relationship, they suggested a functional dependence of the axial stress on the axial displacement, which turns out to be more or less insensitive to the hight of the specimen (Fig. 8). This method of presenting post-peak data is similar to that common in

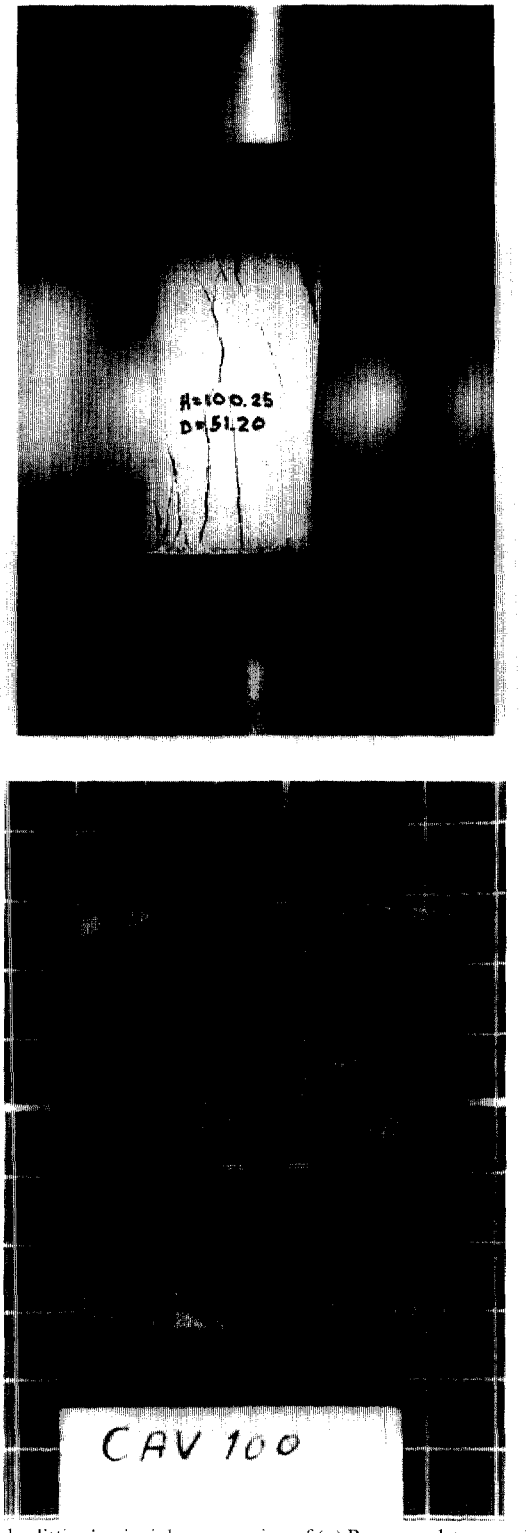


Fig. 5. Failure by 'axial splitting' uniaxial compression of (a) Berea sandstone and (b) Red Wildmoor sandstone (c) Dionysos-Pentelikon marble.


Fig. 5.—*Continued.*

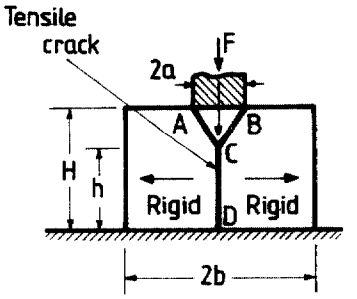


Fig. 6. Reproduction of Chen's (1975) critical splitting mechanism in uniaxial compression (punching).

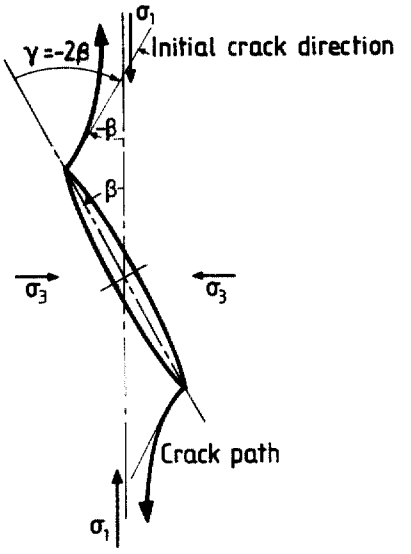


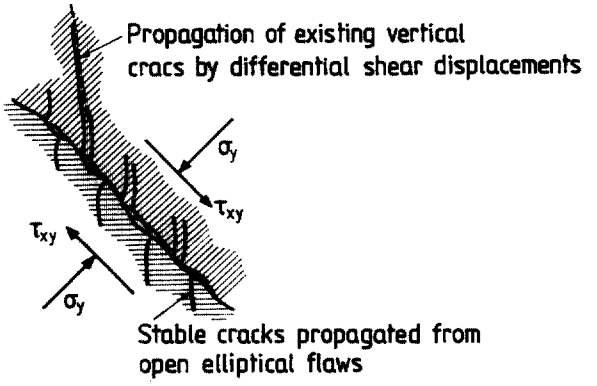


Fig. 7. Reproduction of Hoek's (1968) micromechanical model for axial splitting: (a) direction of crack propagation from the tip of an elliptical flaw under compressive stress conditions. (b) mechanism of fracture propagation by displacement on a shear plane.

soil mechanics evaluation of the direct shear-test. This presentation of test results gave rise to the well known Palmer and Rice (1973) idea of localization of deformation in a shear band (Fig. 9) and to the concept of strain localization and material-length scale, which reflects itself into the shear-band thickness $d_B$ (Vardoulakis and Sulem, 1995). For example,

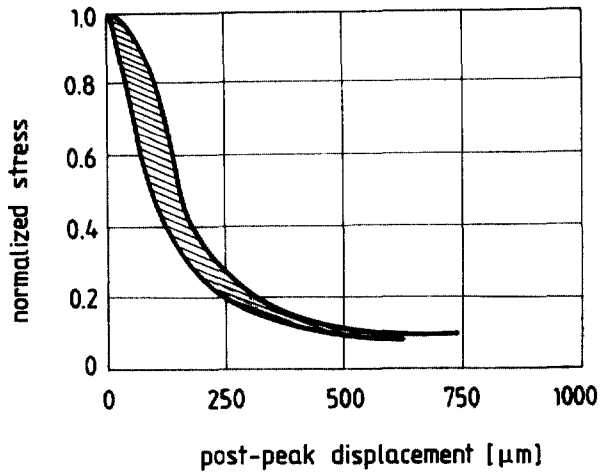


Fig. 8. Reproduction of experimental results of Van Vliet and Van Mier concerning uniaxial compression on plane concrete specimens with lubricated ends.

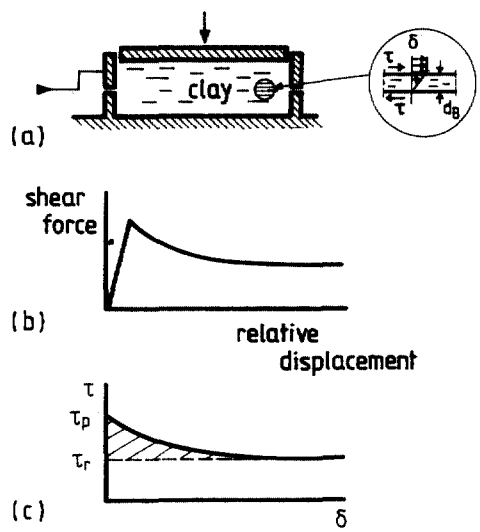


Fig. 9. Reproduction of Palmer and Rice's concept on strain localization in direct shear: (a) Shematic diagram. (b) Relation between shear force and displacement. (c) Relation between shear stress $\tau$ and displacement $\delta$.

using the shear-band thickness as a reference length for the shear displacement $\delta$, a local strain $\gamma = \delta/d_B$ can be introduced, which in turn is independent of the external geometric dimensions of the problem such as the thickness of the layer in direct shear (cf Vardoulakis, 1978; Desrues *et al.* (1991).

The concept of strain localization may not be applicable to the considered problem of uniaxial compression, because there is little evidence of a single localized zone of deformation. As can be seen from Figure 5(a,b,c), there are a few axial cracks visible and at the considered scale we are not able to speak of localization of deformation in a shear band. Thus, to arrive at a continuum description of the observed post-peak phenomena, a new concept that is meant to describe the mechanics of fracture in the uniaxial compression test is needed. Such a continuum, structural theory of fracture in uniaxial compression is presented below.

## 2. EXPERIMENTAL EVIDENCE

In the uniaxial compression test, the specimen is prismatic (usually cylindrical) of height $H$ and diameter $D$. The axial load $F$ is applied on the specimen through a set of rigid

end platens, as shown in Fig. 1. Assuming that the material deforms homogeneously, axial stress $\sigma$ and axial strain $\varepsilon$ are computed from the axial load $F$ and displacement $w$:

$$\sigma = \frac{F}{S} \tag{1}$$

$$\varepsilon = \frac{w}{H} \tag{2}$$

where $S = \pi D^2/4$ is the cross-sectional area of the specimen. As already pointed out by many authors, the continuum mechanics concept of strain, eqn (2), turns out to be useful for the description of the test only up to the point of maximum load $F = F_p$ (p = peak), past which progressive strength reduction and fragmentation of the specimen are observed, and stress-strain curves become meaningless (Van Vliet and Van Mier, 1996). (One may however conceive of several structure models that may in principle be able to account for the applicability of the concept of strain in the post-peak regime. For example, as was pointed out to us by the reviewer of this paper, one may consider the idealized case of separated vertical columns of rock to account for axial splitting. Such and other conceivable structural models that justify the use of strain must be put to test against the experiment. As already mentioned above the experimental results of Van Mier *et al.*, as well as our experimental results do not support such ideas.)

To account for the natural variability of strength within a set of samples from the same batch (which is usually reflected as size effect on peak strength, that is, decrease in strength with increasing volume of sample), Van Vliet and Van Mier (1996) normalized the axial stress by its peak value and plotted it versus the post-peak axial displacement:

$$\tilde{\sigma} = f(\Delta w) \tag{3}$$

where

$$\tilde{\sigma} = \frac{\sigma}{\sigma_p} \tag{4}$$

where

$$\Delta w = w - w_p \tag{5}$$

and $\sigma_p = (\mathrm{UCS})$ is the uniaxial compression strength of the material. This way of presenting the experimental results leads to very good correlations (Fig. 8). In other words, if we plot results this way from uniaxial compression tests on lubricated specimens of the same material, the same diameter but different heights, we obtain practically overlapping normalized stress-displacement curves. It is worth noting, however, that for large displacements the fragmentation of the specimen results in a deterioration of the end platen lubrication, which in turn gives rise to some residual strength. The confinement effect of inavoidable end-platen friction at large displacements is an experimental limitation, which is evident in Fig. 8.

As already introduced, $\sigma$ is a nominal stress, which is evaluated according to eqn (1), for a constant (reference) cross-sectional area of the specimen. Accordingly, the suggestion of Van Vliet and Van Mier (1996) is merely a correlation of the axial load $F = \int \sigma \, \mathrm{d}S$, or of its normalized value

$$\tilde{F} = \frac{F}{F_p} \tag{6}$$

to the post-peak axial displacement $\Delta w$.

The observation of Van Vliet and Van Mier (1996) is corroborated from experiments on different materials as well. In Figure 10(a–d) the post-peak data from uniaxial compression

tests on two rocks and two concretes are plotted. All tests reported here were performed on lubricated cylindrical specimens of 1 : 1 and 2 : 1 height to diameter ratios. Post test examination of the specimens revealed a fracture mode consisting of a set of vertical and sub-vertical fractures for the 1 : 1 ratio specimens, and combinations of vertical and inclined fractures for the 2 : 1 ratio specimens. Figure 11 shows X-ray CT-scan pictures of the tested specimens illustrating the diffuse nature of the failure process.

## 3. DIMENSIONAL ANALYSIS

The post-peak axial load $F$ in a uniaxial compression test will be a function of the mechanical variables of the corresponding boundary-value problem, such as its peak value, the geometric dimensions of the specimen and the applied post-peak displacement.

$$F = f(F_p, H, D, \Delta w, \ldots) \tag{7}$$

where the dots stand for other variables, which are not significant or relevant for the problem at hand and will be disregarded (for instance, Young's modulus or the friction angle of the rock). If we assume that the observed pattern of cracks is completely random, then a discrete material length scale cannot be readily identified. This is for example not the case when microcracks cluster together into shear bands, where one may correlate the shear band thickness to a microstructural length like e.g. the grain size. Accordingly besides $\Delta w$ no other physical property with dimension of length, at this point, enters the argument list of the function $f(.)$ in eqn (7).

One may coin the term continuum fracture mechanics to describe the mechanics of a fragmented medium characterized by a large number of cracks that develop in a relatively small volume in the post-peak regime of a uniaxially compressed brittle-rock specimen. This continuum hypothesis can be justified if indeed the number of cracks in a characteristic volume element is relatively large, so that averages may be taken. First we make the assumption that the failure mechanism is not pure axial splitting; i.e. we assume that fragmentation is characterized by a network of shear and tensile fractures randomly generated and randomly distributed. In this sense the idealized model of perfect columnar structure is far from the case analyzed here. This, however, does not prohibit us from using a concept of an equivalent regular crack array, which has the same total fracture surface as the network of random cracks and which is forming throughout the post-peak phase of a uniaxial compression. In order to support the continuum hypothesis, we use as an example the information which is contained the data plotted in Fig. 10(a–d). In the following we proceed with a rough estimate of the average number of equivalent vertical cracks. We want to emphasize at this point that this estimate of equivalent vertical cracks is not a measure of actually forming vertical cracks. It is rather a piece of information that can be used to support or not support the assumption that in the commonly used specimens in uniaxial compression tests, a 'large' number of cracks are forming. If this is true, continuum mechanics concepts that deal with averages may be used. An estimate of the average number of equivalent vertical cracks in the uniaxial test follows from the work of the applied load

$$W = \int_{w=w_p}^{w_c} F dw \tag{8}$$

First we assume that in the considered case of randomly distributed cracks this work is irreversibly converted into fracture energy

$$W = W_c \tag{9}$$

From the total post-peak fracture energy $W_c$ and the fracture toughness $G_c$ of the considered material we may compute the total fracture surface $S_c$ of the equivalent crack array:

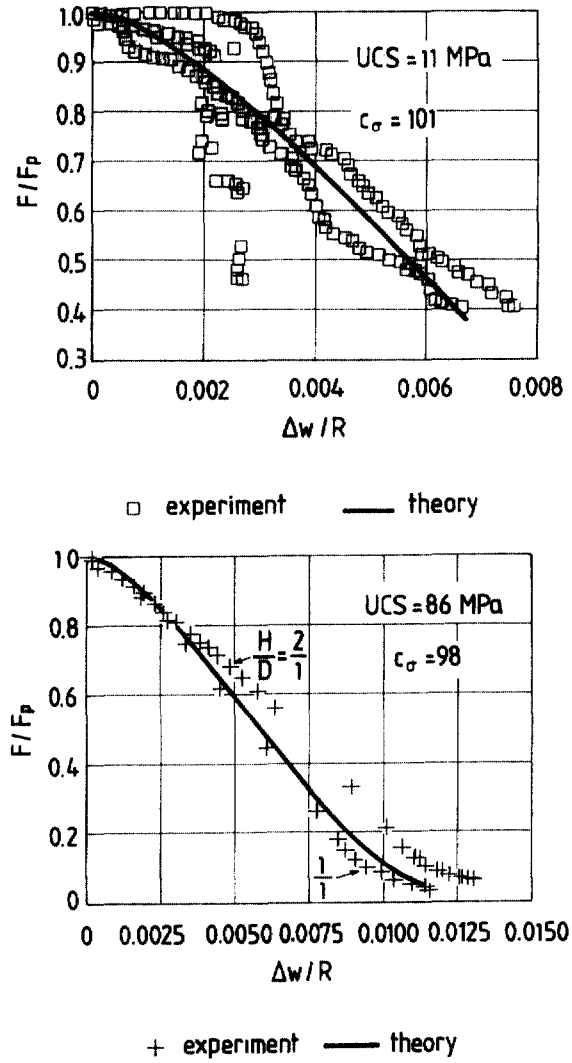


Fig. 10. Post peak normalized stress-displacement curves from uniaxial compression tests: (a) Red Wildmoor sandstone, (b) Dionysos-Pentelicon Marble, (c) High strength concrete (Van Vliet and Van Mier (1966)), (d) concrete (Dasenbrock *et al.* (1995)).

$$S_c = \frac{W_c}{G_c} \tag{10}$$

The experimental evidence summarized in Fig. 10(a–d) leads to the conclusion that: the total fracture energy needed for reaching zero strength in a uniaxial compression of a specimen which is neither too "large" nor too "small" does not depend on the dimensions of specimen. This is an important experimental result which needs of course additional experimental validation. Accordingly, we may say that the experiments suggest that $S_c$ is approximately the same for small and large aspect ratios. However, $S_c$ is large enough to allow a significant population of fractures to develop in both cases. The number of equivalent vertical cracks in a cylindrical specimen with height $H$ and diameter $D$ is computed according to the following equation

$$n = \frac{S_c}{H(\sqrt{\pi}D/2)} \tag{11}$$

For example for the tests on marble (Fig. 10b) we have $W_c = 19$ J and with $G_c = 38$ Jm$^{-2}$,

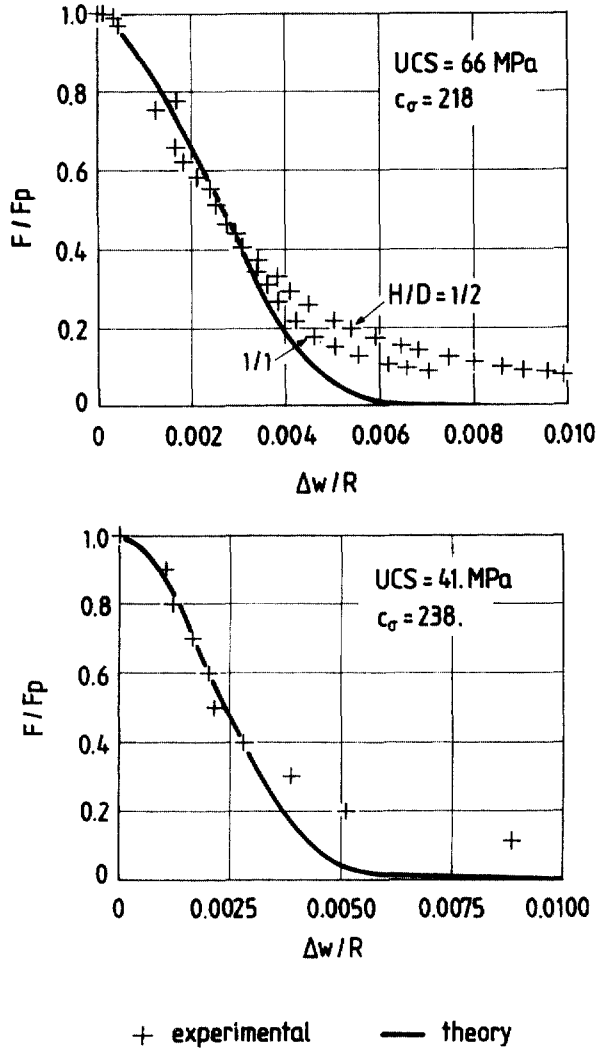


Fig. 10.—*Continued.*

eqn (11) gives the estimate $S_c = 0.5$ m$^2$. For a specimen diameter $D = 45.2$ mm such a calculation gives 276 equivalent vertical cracks for the 1 : 1 specimen and 138 cracks for the 2 : 1 specimen.

On the other hand, analysis of CT images (Fig. 11) and correlation with the rock density allows for a direct estimation of the total fracture volume of the specimen, and thereby the total fracture surface, which for Red Wildmoor sandstone was estimated as follows: (a) For 1 : 1 specimen $S_c = 0.002$ m$^2$, (b) for 1 : 2 specimens $S_c = 0.009$ m$^2$. It should be noted that in these pictures only the major cracks can be captured by the resolution of the CT-scanner which is $0.5 \times 0.5 \times 1.0$ mm, which may partially explain the relatively small value of $S_c$.

Using dimensional analysis the empirical relation (7) can be simplified by introducing appropriate non-dimensional variables: since we are not considering the statistics of strength fluctuations within large masses, the load should be non-dimensionalized by its peak value, eqn (6). In that sense, the experiments suggest that there is no influence of the shape factor (H/D) on the normalized load.

Finally we notice that the experiments reported here as well as the observations made earlier by Van Vliet and Van Mier (1996) suggest that the post-peak data, if presented in terms of the common strain do not collapse in a unique curve. Moreover they do not show any type of dependency or trend as far as the aspect ratio $H/D$ is concerned. Thus, the displacement $\Delta w$ should not be referred as usual to the height $H$ of the specimen, leading

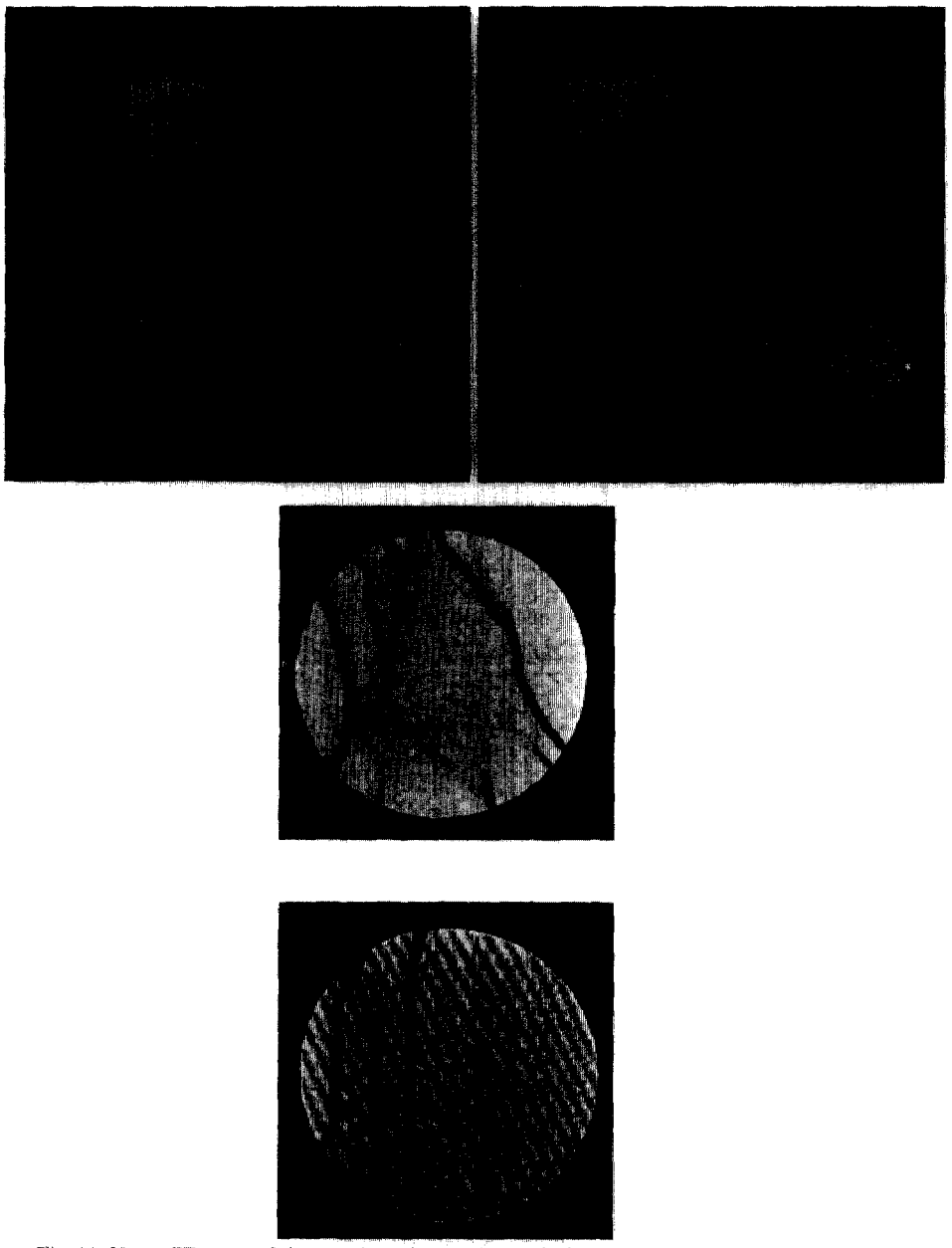

Fig. 11. X-ray CT scans of the tested specimens: (a) vertical sections, and (b) horizontal sections.

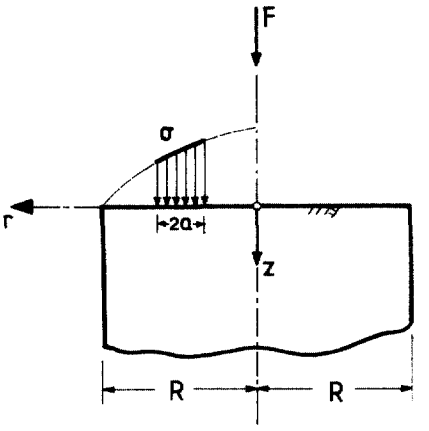


Fig. 12. Assumed post-peak distribution of contact stress in a uniaxial compression test with smooth end platens.

to an exclusion of the common strain $\varepsilon$. Because a unique material length scale, like the grain size (typically reflected in some phenomenon of strain localization), is also excluded from the argument list, a local strain is physically meaningless. This means that $\Delta w$ should be non-dimensionalized by the only remaining property of the problem with dimension of length, namely the diameter or equivalently by the radius, $R = D/2$, of the specimen. These considerations result in the following empirical relation describing post-peak behavior in uniaxial compression of brittle solids:

$$\tilde{F} = \tilde{f}(\tilde{w}) \quad \tilde{w} = \frac{\Delta w}{R} \quad (0 \leqslant \tilde{w} < \infty) \tag{12}$$

We notice $\tilde{w}$ is not a strain measure and accordingly eqn (12) is not a (mean) stress-strain relationship. Consequently, dimensional analysis of the experimental results leads to the conclusion that the observed post-peak strength degradation observed in uniaxial compression of brittle solids cannot be termed as strain-softening as is sometimes done. In the following we present a mathematical model that is free of the concept of strain, and that is capable of describing the experimental findings with a minimum number of parameters.

## 4. POST-PEAK STRESS DIFFUSION

Consider a cylindrical specimen of height $H$ and diameter $D = 2R$ in uniaxial compression and introduce a cylindrical coordinate system $O(r,\theta,z)$, with the $z$-axis coinciding with the axis of the specimen. The platens are smooth and lubricated so that no significant frictional forces may develop at the interfaces. Because the specimen behaves inhomogeneously in the post-peak regime, we assume that the axial load $F_z = F$ is not distributed uniformly over the cross-sectional area of the specimen, resulting in some distribution of the contact stress $\sigma$ in the $z$-direction (Fig. 12). Due to equilibrium in the axial direction, the axial stress at any cross-section is equal to the contact stress at the boundaries, $\partial\sigma_{zz}/\partial z = 0 \Rightarrow \sigma_{zz} = \sigma$. In addition, we assume radial symmetry and allow for the contact stress $\sigma$ to be a function of the radial coordinate $r$. According to the experimental evidence, summarized in eqn (12), the contact stress is assumed to be a function of the (normalized) post-peak axial displacement:

$$\tilde{\sigma} = \tilde{\sigma}(r,\tilde{w}) \quad (0 \leqslant r \leqslant R) \tag{13}$$

In order to arrive at a simple structural model for the post-peak evolution of the contact stress, we test the following set of assumptions:

(A1) at any instant in time and at a given increment of axial displacement, the resulting increment of contact stress at any point of the interface is proportional to the increment of axial displacement, which, due to the rigid platens, is the same for all points of the interface.

This assumption is borrowed directly from Winkler's (Zimmermann, 1888) theory of subgrade reaction, and mathematically can be written as follows:

$$\delta\sigma = k\delta w \tag{14}$$

Notice that Winkler's theory is found to be applicable for a subgrade that is incoherent, that is, without lateral mechanical coupling.

Using non-dimensional variables, eqn (14) becomes

$$\frac{\partial\tilde{\sigma}}{\partial\tilde{w}} = \tilde{k} \qquad \tilde{k} = \frac{k}{\sigma_p/R} \tag{15}$$

holding for $\tilde{w} \geqslant 0$. According to eqn (15) $k \propto 1/R$, i.e. $k$ is inversely proportional to the characteristic dimension of the contact surface.

We remark that in Winkler's original model, $k$ is assumed to be constant and the subgrade is usually depicted as an array of independent elastic springs. Terzaghi (1955) expanded Winkler's concept and, based on model experiments, established that for a plate in contact with a subgrade of infinite extend, $k \propto 1/R^2$. Terzaghi's experimental finding would suggest a modification of the present theory for 'large' specimens where fragmentation will be limited close to the contact surface.

For further determination of the dimensionless coefficient $\tilde{k}$ it is assumed here that,

(A2) $\tilde{k}$ is proportional to the degree of inhomogeneity of the contact stress distribution.

In order to evaluate this assumption, a few terms must be clarified: Using for simplicity cartesian notation, let $\langle\sigma\rangle$ be the local mean value of the stress in a small interval $J = [\xi - a, \xi + a]$ around an arbitrary point $x = \xi$

$$\langle\sigma\rangle = \frac{1}{2a}\int_{\xi-a}^{\xi+a}\sigma(x)\mathrm{d}x$$

Let also $\bar{\sigma}$ be the value of the stress in the midpoint of that interval:

$$\bar{\sigma} = \sigma(\xi)$$

If the function $\sigma(x)$ is constant or varies linearly with $x$ in the considered interval, then from the well known rule of the trapezoid the mean value coincides with value at the midpoint; i.e.

$$\langle\sigma\rangle = \bar{\sigma} \Leftrightarrow \frac{\mathrm{d}^2\sigma}{\mathrm{d}x^2} = 0 \quad \text{for } x \in J$$

In classical continuum mechanics of slow varying fields $\bar{\sigma} = \sigma(\xi)$ is always identified with its local average $\langle\sigma\rangle$. In this case, the field $\sigma(x)$ is called locally homogeneous. This condition is assumed to be true prior to peak load, when the axial load is assumed to be, within a good approximation, homogeneously distributed, and accordingly the stress $\sigma$ is set constant over the contact area; cf. eqn (1)

$$\sigma = \frac{F}{S} = \langle\sigma\rangle = \text{const.}$$

In the post-peak regime, this assumption is relaxed. This is because we recognise that the contact stress may not be constant over the contact area. In this case $\langle\sigma\rangle$ may differ from

its local value $\bar{\sigma}$ by a significant term, which accounts for the spatial variability of the considered field. It can be easily shown that in this case the following numerical midpoint integration rule for the computation of $\langle\sigma\rangle$ holds,

$$\langle\sigma\rangle = \frac{1}{2a}\int_{-a}^{a}\sigma(\xi+h)\mathrm{d}h = \frac{1}{2a}\int_{-a}^{a}\left\{\sigma(\xi)+h\left.\frac{\mathrm{d}\sigma}{\mathrm{d}x}\right|_{x=\xi}+\frac{1}{2}h^2\left.\frac{\mathrm{d}^2\sigma}{\mathrm{d}x^2}\right|_{x=\xi}+\ldots\right\}\mathrm{d}h$$

$$= \bar{\sigma}+\frac{a^2}{12}\left(\frac{\mathrm{d}^2\sigma}{\mathrm{d}x^2}\right)_{x=\xi}+O(a^4)$$

This rule can be generalized in 2 or 3 dimensions (Vandoulakis and Sulem, 1995), and takes the form,

$$\langle\sigma\rangle = \bar{\sigma}+l^2\nabla^2\sigma\Big|_{x=\xi}+O(l^4) \tag{16}$$

where $\nabla^2$ is the Laplacian operator and $l$ is proportional to the radius, $a$, of the domain over which the averaging is done. We emphasize that in this case the averaging is not done over the whole cross-sectional area of the specimen, as is the case in the pre-peak phase, but over a smaller area around a given point in the contact area, say of radius $a \ll R$.

According to (A2) we assume that the coefficient $\tilde{k}$ is proportional to the degree of inhomeneity, which in view of the above remarks means that it must be set proportional to the difference $\langle\sigma\rangle-\bar{\sigma}$. In view of eqn (16), and since the coefficient $l^2$ is not specified at this point we may assume that

$$\tilde{k} = \langle\tilde{\sigma}\rangle-\tilde{\bar{\sigma}} = l^2\nabla^2\tilde{\sigma}\Big|_{x=\xi} \tag{17}$$

Combining eqns (15) and (17) yields the following partial differential equation for the evolution of the contact stress in the post-peak regime:

$$\frac{\partial\tilde{\sigma}}{\partial\tilde{w}} = l^2\nabla^2\tilde{\sigma} \tag{18}$$

The length $l$ must depend on a characteristic length of the network of randomly distributed cracks that develop in the post-peak regime through a continuous process of crack propagation and crack bifurcation. We distinguish here among three possibilities:

(a) There is a unique characteristic length scale $l_c$, like the mean crack length of normally distributed crack lengths which in turn may be determined by the grain size $D_g$. In this case micro-cracks may not extend more than one grain diameter, and we may assume that

$$l = cD_g \tag{19a}$$

(b) There is no discrete crack length, but rather a continuous spectrum of crack lengths. In this case the characteristic length must correlate to the only evolving property of the problem with dimension of length, namely to the applied displacement itself, $\Delta w = \int dw$, leading to the assumption that

$$l = c\Delta w \tag{19b}$$

(c) Intermediate conditions are also possible, like

$$l = c\sqrt{(D_a \Delta w)} \tag{19c}$$

In the above equations $c$ is a dimensionless constant. Which of the above assumptions is correct, is a "matter for the experimental test" to decide. Here the analysis of the considered data justified assumption (19b).

The governing eqn (18) with (19b) can be further simplified by introducing the dimensionless radial coordinate:

$$\rho = \frac{r}{R} \quad (0 \leqslant \rho \leqslant 1) \tag{20}$$

resulting in

$$\frac{\partial \tilde{\sigma}}{\partial \tilde{w}} = c\tilde{w}^2 \nabla_\rho^2 \tilde{\sigma} \tag{21}$$

where

$$\nabla_\rho^2 = \frac{1}{\rho}\frac{\partial}{\partial \rho}\left(\rho \frac{\partial}{\partial \rho}\right)$$

is the Laplacian operator in polar coordinates and axisymmetric conditions.

The dimensionless displacement is rescaled by using the only free parameter of the problem

$$s = c_\sigma \tilde{w} \qquad c_\sigma = c^{1/3} \tag{22}$$

Accordingly, the governing differential eqn (18) transforms into a universal diffusion-type, partial differential equation for the normalized stress:

$$\frac{\partial \tilde{\sigma}}{\partial s} = s^2 \nabla_\rho^2 \tilde{\sigma} \tag{23}$$

In this equation the rescaled, normalized axial displacement $s$ plays the role of time, which has to be understood as follows: The incompatibility of boundary displacement and the tendency of the material towards axial cracking drives the generation of randomly oriented cracks, which in turn result in net strength degradation. The displacement is the same for all points in the cross-section, and according to eqn (19b) the average micro-crack length is proportional to the displacement; the dimensionless correlation coefficient $c_\sigma = \sqrt[3]{c}$, must be fitted from the experimental data, and it may be different for various brittle solids.

Formally the considered process may be called a phenomenon of stress diffusion, which is resulting from the post-peak fragmentation of the specimen. Obviously, if the stress is homogeneously distributed over the cross section of the specimen, then $\langle \sigma \rangle - \bar{\sigma} = 0$, and no stress-diffusion is taking place. This new concept of stress diffusion due to microcracking is introduced here to replace the concept of stress-strain softening, which, as already mentioned, is not applicable because no localization of the damage process is observed.

The initial, boundary-value problem of post-peak stress diffusion due to material fragmentation is now posed as follows: The stress obeys diffusion eqn (23) with the following initial condition

$$\tilde{\sigma} = 1 \text{ for } s = 0 \quad \text{and} \quad 0 \leqslant \rho \leqslant 1 \tag{24}$$

Equation (24) reflects the fact that up to peak load the assumption of homogeneous stress distribution along the cross section is holding.

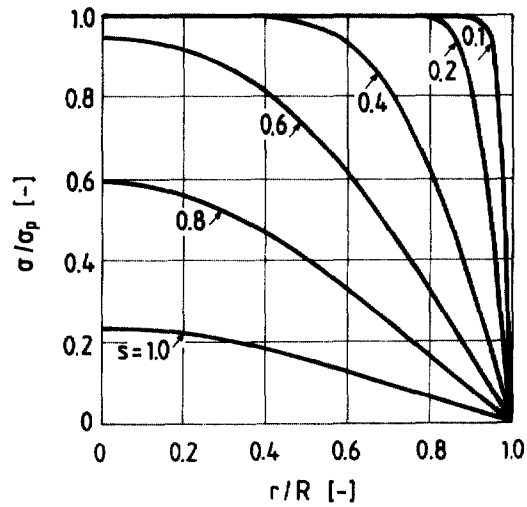


Fig. 13. Theoretical distribution of normalized contact stress at various rescaled normalized displacements.

In order to establish the necessary boundary condition we argue as follows: Due to random crack formation, edges of a specimen break away and lose first the ability to carry load resulting to the following "natural" boundary condition:

$$\tilde{\sigma} = 0 \quad \text{for } s > 0 \quad \text{and } \rho = 1 \tag{25}$$

Equations (23)–(25) are solved analytically by separation of variables technique and by Fourier-Bessel series expansion of the initial condition (24). The resulting expression for the contact stress is

$$\tilde{\sigma} = 2 \sum_{k=1}^{\infty} \frac{J_0(\lambda_k \rho)}{\lambda_k J_1(\lambda_k)} exp(-\lambda_k^2 s^3/3) \tag{26}$$

where $J_0$ and $J_1$ are Bessel functions of zero and first order, and $\lambda_k$ are the zeros of $J_0$ (cf. Abramowitz and Stegun, 1964):

$$J_0(\lambda_k) = 0 \quad \lambda_1 < \lambda_2 < \cdots \quad (\lambda_1 = 2.40482\cdots, \lambda_2 = 5.52008\cdots, \cdots) \tag{27}$$

Figure 13 shows the 'isochrones' computed from eqn (26) for various characteristic values of the time-like factor $s$. Integrating (26) leads to the expression of the normalized axial load:

$$\tilde{F} = 4 \sum_{k=1}^{\infty} \frac{1}{\lambda_k^2} \exp(-\lambda_k^2 s^3/3) \tag{28}$$

This universal formula for the post-peak evolution of the axial load can be used for validating the theory and for fitting the correlation parameter $c_\sigma$. The theoretical curve given by equation (28) may be approximated by the following,

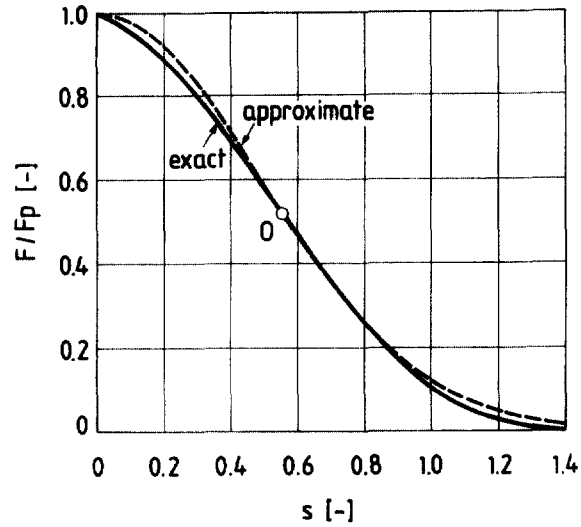


Fig. 14. Theoretical non-dimensional load-displacement curve.

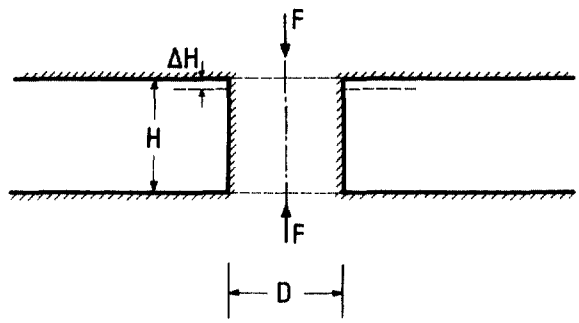


Fig. 15. Application example on the bearing capacity of a mine pillar.

$$\tilde{F} \approx \exp(-2.1 s^2) \tag{29}$$

As shown in Fig. 14 the predicted load-displacement curve is bell-shaped, similar to the experimentally determined ones of Figs 8, 10. It turns out that if the experiment yields a straight line, then assumption (19c) is more applicable. Finally we should mention that in case of a concave curve, assumption (19a) should be used.

## 5. ANALYSIS AND DISCUSSION

For the calibration of the above one-parameter theoretical model, the scaling parameter $c_\sigma$ is fitted at a single point of the experimental curves. As a fitting point, the inflection point O in Fig. 14 of the bell-shaped was the selected curve with

$$s_0 = 0.5560 \qquad \tilde{F}_0 = 0.5202 \tag{30}$$

In Table 1, the uniaxial compression strength, $\sigma_p$, and the corresponding value of the correlation parameter $c_p$ are given for the considered solids. The analysis of the experimental data using eqn (28) and the value $c_\sigma$ from Table 1 are depicted in Fig. 10(a–d) as a solid line, together with the experimental data. From these figures follows the justification of the present continuum theory of post-peak continuum fracture mechanics of rocks in uniaxial compression.

In order to discuss the physical (macroscopic) meaning of the (dimensionless) parameter $c_\sigma$, the total fracture energy is computed:

Table 1. Characteristic material properties

| | $\sigma_p$ [MPa] | $c_\sigma$ [–] | $\sigma_p/c_\sigma$ [MPa] |
|---|---|---|---|
| Sandstone ([28] $D = 50$ mm | 11 | 105 | 0.1 |
| Marble ([11] $D = 45$ mm) | 86 | 98 | 0.9 |
| Concrete ([29] $D = 94$ mm) | 66 | 216 | 0.3 |
| Concrete )[24] $D = 113$ mm) | 41 | 238 | 0.2 |

$$W^c = \int \mathrm{Fdw} = \kappa \frac{\pi D^2 \sigma_p}{4\ c_\sigma} D \tag{31}$$

where $\kappa$ is a number resulting from the integration of $\tilde{F}$ from eqn (28):

$$\kappa = \frac{2}{3}\Gamma(1/3) \sum_{k=1}^{\infty} \lambda_k^{-8/3} \simeq 0.2934. \tag{32}$$

We define the contact surface-specific fracture energy $f_c$, that is, the total fracture energy referred to the cross-sectional area of the specimen:

$$f_c = \frac{W_c}{\pi D^2/4} \tag{33}$$

From eqns (31) to (33) we get

$$f_c \approx 0.3 \frac{\sigma_p}{c_\sigma} D \tag{34}$$

which is a formula for estimating the total fragmentation energy of a prismatic solid under uniaxial compression, whose base has an equivalent diameter $D$. From this expression it follows that $c_\sigma$ is a measure of continuum brittleness (the larger $c_\sigma$ the more brittle is the specimen). Accordingly, the two rocks analyzed above are equally brittle. However, marble is more resistant to fragmentation than sandstone, since $\sigma_p/c_\sigma$ is larger. On the other hand, the two types of concrete discussed are found to be equally brittle. If $c$ turns out to be independent of $D$, then eqn (34) predicts a scale effect, which in view of its possible practical importance (for example in rock fragmentation) deserves further experimental validation. Notice that in all reported experiments, the diameter of the specimen was kept the same and only the height was varied.

*Application*

As a practical application of the present theory, consider the problem of the bearing capacity of a pillar in a deep mine (Fig. 15). To assess the bearing capacity of the deep-mine pillar, one should first establish a reference state (height $H_p$ and diameter $D_p$) of the pillar where the peak load $F = F_p$ has been reached. This can be done by an elastic stress analysis, which is quite adequate in the pre-peak regime (Crouch and Stanfield, 1983). Past this state, an elastic analysis is not applicable; convergence $\Delta H$ of the stope and the reduction in pillar diameter due to mining should be monitored in situ. Let $D_p$ be the current value of the pillar diameter. At any instant, the bearing capacity of the pillar can be estimated from the following expression:

$$F = \tilde{F}(s)F_p\,;\, F_p = \sigma_p(\pi D^2/4) \tag{35}$$

Where $\tilde{F}$ is computed from eqn (29). It should be noticed finally that the uniaxial compression strength $\sigma_p$ and the continuum brittleness $c_s$ of the rock should be determined in the laboratory using a small number of displacement-controlled, uniaxial compression tests with lubricated platens.

*Acknowledgements*—The authors wishes to thank (a) the E.U. EV Program (EV 5V CT93-300) and SMT Program (SMT4-CT96-2130), (b) the University of Minnesota M.T.S. Systems Visiting Professorship and (c) the consortium of Oil companies consisting of Agip, Conoco, Elf, Hydro, Saga, Shell, Statoil, for supporting this research on the mechanical properties of marble and sandstone.

## REFERENCES

Abramowitz, M. and Stegun, I. (1964) *Handbook of Mathematical Functions*. Dover.

Bell, J. F. (1973) The Experimental Foundations of Solid Mechanics. In *Encyclopedia of Physics*. Vol. VIa/1, Sect. 3.3, Springer Verlag.

Brace, W. F. and Bombolakis, E. G. (1963) A note on brittle crack growth in compression. *J. Geophys Res.* **68**, 3709–3713.

Chau, K. T. (1993) Anti-symmetric bifurcations in a compressible pressure-sensitive circular cylinder under axisymmetric tension and compression. *J. Appl. Mech.* **60**, 282–289.

Chen, Wai-Fa (1975) *Limit Analysis and Soil Plasticity*. Elsevier.

Crouch, S. L. and Starfield, A. M. (1983) *Boundary Element Methods in Solid Mechanics. George Allen & Unwin, London.*

*Dasenbrock, D., Labuz, J. F. and French, C. W.* (1995) *Strain softening of concrete in uniaxial compression. Final report to RILEM committee* 148-*sec, University of Minnesota.*

*Desrues, J., Mokni, M. and Mazerolle, F.* (1991) *Tomodensitom. trie et la localisation sur les sables.* 10*th E.C.S.M.F.E.*, 61–64.

*Drescher, A. and Vardoulakis, I.* (1982) *Geometric softening in triaxial test on granular materials. Geotechnique* **32**, 291–303.

Fairhurst, C. and Cook, N. G. W. (1966) The phenomenon of rock splitting parallel to the direction of maximum compression in the neighborhood of a free surface. In *Proc. 1st Congr. Int. Soc. Rock Mech., Lisbon* **1**, 687–692.

Hoek, E. and Bieniawski, Z. T. (1965) Brittle fracture in rock under compression. *Int. J. Rock Mech. Min. Sci. and Geomech. Abstr.* **10**, 713–726.

Hoek, E. (1968) Brittle failure of rock. In *Rock Mechanics in Engineering Practice*, ed. K. G. Stagg and O. C. Zienkiewicz, pp. 99–124. John Wiley.

Horii, H. and Nemat-Nasser, S. (1986) Brittle failure in compression: Splitting, faulting and brittle-ductile transition. *Phil. Trans. R. Soc. Lond.* **A.319**, 337–374.

Hudson, J. A., Brown, E. T. and Fairhurst, C. (1971), Shape of complete stress-strain curve for rock. *Proc. 13th Symp. on Rock Mechanics*, University of Illinois, Urbana, III.

Labuz, J. F. and Bridell, J. M. (1993) Reducing frictional constraint in compression testing through lubrication. *Int. J. Rock Mech. Min. Sci. and Geomech. Abstr.* **30**, 451–455.

Michalowski, R. L. (1985) Limit analysis of quasi-static pyramidal indentation of rock. *Int. J. Rock Mech. Min. Sci & Geomech. Abstr.* **22**, 31–38.

Mohr, O. (1900) Welche Umstaendnde Bedingen die Elastizitaetsgrenze und den Bruch eines Materials? *Zeitschrift des Vereines deutscher Ingenieure* **44**, 1–12.

Okui, Y. and Horii, H. (1995) A micromechanics-based continuum theory for microcracking lokalization of rocks under compression. In *Continuum Models for Materials with Microstructure*, pp. 27–66, Wiley.

Palmer, A. C. and Rice, J. R. (1973) The growth of slip surfaces in progressive failure of over-consolidated clay. *Proc. Roy. Soc. Lond.* **A.332**, 527–548.

Papamichos, E., Labuz, J. F. and Vardoulakis, I. (1994) A surface instability detection apparatus. *Rock Mech. and Rock Enrng.* **27**, 37–56.

Papamichos, E., Tronvoll, J., Vardoulakis, I. and Sulem, J. (1995) Investigation of cavity failures for sand production—Phase II. IKU Technical Report.

Read, H. E. and Hegemier, G. A. (1984) Strain softening of rock, soil and concrete—A review article. *Mechanics of Materials* **3**, 271–294.

Schlangen, E. and Van Mier, J. G. M. (1994), Fracture simulations of concrete and rock using a random lattice. In *Computer Methods and Advances in Geomechanics*, ed. H. J. Siriwardane and M. M. Zaman, pp. 1641, Balkema.

Shah, K. R. and Labuz, J. F. (1995) Damage mechanisms in stressed rock from acoustic emission. *J. Geophys. Res.* **100**(B8), 15,527–15,539.

Sulem, J. and Vardoulakis, I. (1990) Bifurcation analysis of the triaxial test on rock specimens. A theoretical model for shape and size effect. *Acta Mechanica* **83**, 195–212.

Terzaghi, K. V. (1955) Evaluation of coefficients of subgrade reaction. *Geotechnique* **5**, 297–326.

Van Vliet, M. R. A. and Van Mier, J. G. M. (1996) Experimental investigation of concrete fracture under uniaxial compression. *Mech. of Cohesive-Frictional Materials* **1**, 115–127.

Vardoulakis, I. (1978) Equilibrium bifurcation of granular earth bodies. In *Adv. Anal. Geotech. Instabilities*, 13, pp. 65–120. Univ. of Waterloo Press.

Vardoulakis, I. and Papamichos, E. (1991) Surface instabilities in elastic anisotropic media with surface-parallel Griffith cracks. *Int. J. Rock mech. Min. Sci. and Geomach. Abstr.* **28**, 163–173.
Vardoulakis, I., Exadaktylos, G. and Kourkoulis, S. K. (1998) A gradient theory with surface energy and size effects. *J. de Physique IV*, in print.
Vardoulakis, I. and Sulem, J. (1995) *Bifurcation Analysis in Geomechanics*. Blackie Academic and Professional.
Waversik, W. R. (1968) Detailed analysis of rock failure in laboratory compression tests. Ph.D Thesis University of Minnesota.
Zimmermann, H. (1888) *Die Berechnung des Eisenbahn-Oberbaues*. Ernst, Berlin.